Molecular and Cellular Biology

Hereditary Inclusion Body Myopathy-Linked p97/VCP Mutations in the NH$_2$ Domain and the D1 Ring Modulate p97/VCP ATPase Activity and D2 Ring Conformation

Dalia Halawani, Andréa C. LeBlanc, Isabelle Rouiller, Stephen W. Michnick, Marc J. Servant and Martin Latterich

Mol. Cell. Biol. **2009, 29(16):4484. DOI: 10.1128/MCB.00252-09.**
Published Ahead of Print 8 June 2009.

MOLECULAR AND CELLULAR BIOLOGY, Aug. 2009, p. 4484–4494 Vol. 29, No. 16
0270-7306/09/$08.00+0 doi:10.1128/MCB.00252-09

Hereditary Inclusion Body Myopathy-Linked p97/VCP Mutations in the NH_2 Domain and the D1 Ring Modulate p97/VCP ATPase Activity and D2 Ring Conformation▽

Dalia Halawani,[1] Andréa C. LeBlanc,[2] Isabelle Rouiller,[1] Stephen W. Michnick,[3] Marc J. Servant,[4] and Martin Latterich[1,4]*

Department of Anatomy and Cell Biology, McGill University, 3640 University Street, Montréal, Québec H3T 1E2,[1] Department of Neurology and Neurosurgery, McGill University, 3801 University Street, Montréal, Québec H3A 2B4,[2] Département de Biochimie, Université de Montréal Casier Postal 6128, Succursale Centre-Ville, Montréal, Québec H3C 3J7,[3] and Faculty of Pharmacy, Université de Montréal, Montréal, Québec H3T 1J4,[4] Canada

Received 25 February 2009/Returned for modification 6 April 2009/Accepted 29 May 2009

Hereditary inclusion body myopathy associated with early-onset Paget disease of bone and frontotemporal dementia (hIBMPFTD) is a degenerative disorder caused by single substitutions in highly conserved residues of p97/VCP. All mutations identified thus far cluster within the NH_2 domain or the D1 ring, which are both required for communicating conformational changes to adaptor protein complexes. In this study, biochemical approaches were used to identify the consequences of the mutations R155P and A232E on p97/VCP structure. Assessment of p97/VCP oligomerization revealed that $p97^{R155P}$ and $p97^{A232E}$ formed hexameric ring-shaped structures of ~600 kDa. $p97^{R155P}$ and $p97^{A232E}$ exhibited an ~3-fold increase in ATPase activity compared to wild-type p97 ($p97^{WT}$) and displayed increased sensitivity to heat-induced upregulation of ATPase activity. Protein fluorescence analysis provided evidence for conformational differences in the D2 rings of both hIBMPFTD mutants. Furthermore, both mutations increased the proteolytic susceptibility of the D2 ring. The solution structures of all p97/VCP proteins revealed a didispersed distribution of a predominant hexameric population and a minor population of large-diameter complexes. ATP binding significantly increased the abundance of large-diameter complexes for $p97^{R155P}$ and $p97^{A232E}$, but not $p97^{WT}$ or the ATP-binding mutant $p97^{K524A}$. Therefore, we propose that hIBMPFTD p97/VCP mutants $p97^{R155P}$ and $p97^{A232E}$ possess structural defects that may compromise the mechanism of p97/VCP activity within large multiprotein complexes.

The ubiquitous *v*alosin-*c*ontaining *p*rotein (p97/VCP) is a prominent member of the highly conserved AAA^+ (*A*TPases *a*ssociated with diverse cellular *a*ctivities) proteins, which are known for their oligomeric structure and chaperone-like activities. p97/VCP is an essential biochemical component of a wide range of ubiquitin-linked cell biological reactions, including ubiquitin-proteasome system-mediated protein degradation (8), Golgi and endoplasmic reticulum (ER) membrane fusion (1, 18), transcription factor activation (19), and DNA repair (10, 16). In these processes, p97 acts as a molecular segregase that utilizes ATP-powered conformational changes in the assembly and disassembly of macromolecular machineries (8, 11).

p97 ATPase activity is contingent on the assembly of an inherently stable hexamer (24) comprised of two highly homologous D1 and D2 nucleotide-binding rings and regulatory NH_2- and COOH-terminal domains (4). ATP hydrolysis in the D2 ring mediates p97 major ATPase activity, while the D1 ring is involved in the regulation of p97 hexamerization (24). Recently, p97 has been linked to a severe degenerative disorder identified as *h*ereditary *i*nclusion body *m*yopathy associated with early-onset *P*aget disease of bone and *f*ronto*t*emporal *d*ementia (hIBMPFTD). The pathogenesis of hIBMPFTD is attributed to autosomal-dominant single-amino-acid substitutions in highly conserved residues within the p97 NH_2 domain and D1 ring (28). Patients present with hallmark features of a "protein conformational" disorder in which proteinaceous inclusions accumulate in the cytoplasm and nuclei of degenerating myofibrils (13) and dystrophic neurites (7, 15, 23). Transgenic expression of hIBMPFTD p97 mutants in a murine model sufficiently recapitulates these inclusions (31). While the ultrastructure and composition of hIBMPFTD inclusions are poorly defined, several reports have identified p97/VCP and ubiquitin as major constituents (12, 28, 32). Furthermore, overexpression of hIBMPFTD mutants in C2C12 skeletal myoblasts results in p97 localization to cytoplasmic inclusions and fractionation with insoluble proteins (30). One possibility is that misfolding or misassembly directly mediates p97/VCP accumulation in inclusion bodies, which in turn nucleates the entrapment of its interacting proteins. Alternatively, the biogenesis of p97-containing inclusions could represent an indirect consequence of failure in other p97/VCP-dependent pathways upstream of the ubiquitin-proteasome system. The mechanisms by which hIBMPFTD p97 mutants induce the biogenesis of inclusion bodies in cell culture models are not well understood (9, 30).

Despite current progress in resolving more refined p97/VCP crystal structures in various nucleotide-binding states (3, 5), clues about how hIBMPFTD mutations impact p97 structure or conformation remain elusive. Cryo-electron microscopy (cryo-EM)

* Corresponding author. Present address: The Nicholas Conor Institute for Pediatric Cancer Research, 9710 Scranton Road, Suite 170, San Diego, CA 92121. Phone: (858) 353-9667. Fax: (858) 450-9834. E-mail: mlatterich@gmail.com.

▽ Published ahead of print on 8 June 2009.

(21, 22) and crystallography studies (4, 5) of p97 in various nucleotide-binding states have revealed extensive communication between the tripartite NH_2-D1-D2 domains (17). Conformational changes first initiated in the D2 ring are relayed through a D1-D2 linker region to the D1 α-helical subdomain. The D1 α-helical subdomain in turn communicates these motions to the flexibly linked NH_2 domain, thereby regulating its conformation (5). Ultimately, these ATP-powered conformational changes are utilized in remodeling macromolecular complexes. One hypothesis is that hIBMPFTD mutations interfere with p97/VCP biochemical activity by altering its conformation or interdomain communication. For example, structural analysis of p97/VCP in the preactivated ATP-occupied state revealed communication between Arg^{155} and Arg^{159} within the NH_2-terminal domain and the D1 residue Asn^{387}, all of which are now identified as mutated residues in hIBMPFTD (5, 9). However, it remains to be seen whether hIBMPFTD mutations do indeed induce structural or conformational defects in p97/VCP.

In this report, we specifically focused on studying hIBMPFTD $p97^{R155P}$ and $p97^{A232E}$ mutants because Arg^{155} is the most commonly affected amino acid residue and mutation of Ala^{232} is associated with increased severity of the disease (13, 28). A series of biochemical approaches were employed to characterize the oligomeric assembly, ATPase activity, and solution structure of wild-type ($p97^{WT}$) and mutant p97. Our results indicate that recombinant $p97^{R155P}$ and $p97^{A232E}$ assembled into ~600-kDa complexes, similar to $p97^{WT}$. Both mutants showed a threefold increase in ATPase activity and increased sensitivity to heat-induced upregulation in ATPase activity. Analysis of the intrinsic protein fluorescence and proteolytic susceptibility provided evidence for conformational defects in the D2 ring. These effects were correlated with increased propensity for aggregation in the presence of ATP. Based on these data, we propose that hIBMPFTD p97 mutations induce structural defects, which may underlie the mechanism of pathogenesis in biological systems.

MATERIALS AND METHODS

Generation of p97/VCP recombinant expression constructs. A wild-type murine p97 cDNA clone in pBluescript SK(+) was a kind gift of Fred Indig (National Institute on Aging, NIH, Baltimore, MD). To introduce hIBMPFTD mutations, p97cDNA was subjected to site-directed mutagenesis using the GeneTailor kit according to the manufacturer's instructions (Invitrogen, Carlsbad, CA). For the R155P mutation, G^{464} in codon $^{463}CGG^{465}$ was replaced with C using the following primers: 5′ AGGAGATATTTTTCTTGTCCCGGGTGGGATG 3′ and 5′ GGACAAGAAAAATATCTCCTTTACGGATGGGCC 3′. For the A232E mutation, C^{695} in codon $^{694}GCG^{696}$ was mutated to A using primers 5′ ACATCC TGCGCTCTTCAAGGAGATTGGTGTA 3′ and 5′ CCTTGAAGAGCGCAGG ATGTCTCAGTGGCAGCT 3′. cDNA of the ATP-binding-deficient mutant $p97^{K524A}$ in the pQE9 vector was a kind gift from T. Rapoport (Harvard University, Cambridge, MA). Subsequently, all constructs were subcloned into the pTrcHis2C vector backbone (Invitrogen, Carlsbad, CA) for COOH-terminal polyhistidine tagging by PCR. Briefly, cDNA was amplified using the primers 5′ CCGAGCTCGG CCTCTGGAGCCGAT 3′ and 5′ ATGGTACCAGCGGCATACAGGTCATC 3′, which contained SacI and KpnI restriction sites, respectively. Following restriction digestions, the PCR products were ligated into the pTrcHis2C multiple-cloning site. Insertion of the cDNA was verified by restriction digestion, which was followed by full sequencing (McGill University and Genome Quebec Innovation Center, Montreal, Canada).

Expression and purification of recombinant p97/VCP. $p97^{WT}$ and mutant variants were expressed in the TOP10 *Escherichia coli* strain. Overnight starter cultures were diluted 50-fold in 2 liters of 2× YT medium (16 g/liter tryptone, 10 g/liter yeast extract, 5 g/liter NaCl) with 100 μg/ml ampicillin and grown at 37°C until they reached an optical density at 600 nm of 0.6. The cultures were subsequently induced with 300 μM IPTG (isopropyl-β-D-thiogalactopyranoside) and grown for another 4 h. The cells were pelleted by centrifugation (4,000 × *g* for 20 min) and lysed in buffer A (20 mM HEPES, pH 7.5, 300 mM NaCl, 5 mM $MgCl_2$, 2.5 mM dithiothreitol [DTT], and 20 mM imidazole) supplemented with 1 mg/ml lysozyme and complete protease inhibitors (Roche, Mississauga, Canada). Following sonication, the lysates were cleared by centrifugation at 26,000 × *g* for 45 min. The supernatant was then loaded on a 5-ml Ni^{2+} affinity column (GE Healthcare Biosciences, Uppsala, Sweden) preequilibrated with 10 column volumes of buffer A. Following a first wash with 10 column volumes of buffer A, bound proteins were subjected to an additional wash with 10 column volumes of buffer B (20 mM HEPES, pH 7.5, 300 mM NaCl, 5 mM $MgCl_2$, 2.5 mM DTT, and 35 mM imidazole). The proteins were eluted with a 35 to 500 mM imidazole gradient over 5 column volumes. Peak fractions containing p97 were pooled, concentrated on an Amicon Ultra column (molecular mass cutoff, 15,000 kDa), and loaded on a precalibrated 100-ml Superose-6 gel filtration column (GE Healthcare Biosciences, Uppsala, Sweden). Size-fractionated proteins were eluted as 1-ml fractions in buffer C (20 mM HEPES, pH 7.5, 150 mM NaCl, 5 mM $MgCl_2$, and 2.5 mM DTT). All purifications were performed at 4°C using the UKTA fast-performance liquid chromatography purification system (GE Healthcare Biosciences, Uppsala, Sweden). Protein concentrations were determined using the Bradford assay (Bio-Rad, Mississauga, Canada).

Native gel electrophoresis. Ten micrograms of purified recombinant $p97^{WT}$ or mutant variants was loaded on a 6% Tris-polyacrylamide gel (pH 8.0). Electrophoresis was performed at 4°C using 200 V and ice-cold 1× Tris-glycine buffer (pH 8.0) to prevent heat-induced denaturation.

Negative-staining EM. p97 proteins were diluted to a concentration of 50 μg/ml in buffer containing 20 mM HEPES, pH 7.5, 150 mM NaCl, 10 mM $MgCl_2$, and 1 mM DTT in the presence or absence of 1 mM ATP (Sigma, Oakville, Ontario, Canada). For each protein, a 5-μl sample was spotted on a glow-discharged carbon-coated copper grid. The grids were then stained for 60 s with 5 μl of uranyl acetate and visualized using an FEI Tecnai 12 120-kV electron microscope. Digital images were collected with a Gatan 792 Bioscan 1,000 by 1,000 wide-angle multiscan charge-coupled device camera. Images were cropped at the level of the scale bar to show ~25% of the full image.

Dynamic-light-scattering (DLS) measurements. p97 protein samples were diluted to 100 μg/ml in buffer containing 20 mM HEPES, pH 7.5, 150 mM NaCl, 10 mM $MgCl_2$, and 1 mM DTT in the presence or absence of 2 mM ATP. Measurements were performed using the Zetasizer Nano ZS (Malvern) at 20°C.

ATPase activity assays. p97 ATPase activity was assessed using the EnzCheck phosphate assay kit (Molecular Probes, OR) as previously described (6). This assay is based on the inorganic-phosphate-dependent conversion of 2-amino-6-mercapto-7-methylpurine riboside to ribose-1-phosphate and 2-amino-6-mercapto-7-methylpurine, which results in a shift of the maximum absorbance from 330 nm to 360 nm (29). For assessment of p97 ATPase activity, 50 nM of p97 (based on the ~600-kDa hexamer) was incubated in 100 μl reaction buffer (20 mM HEPES, pH 7.5, 150 mM NaCl, and 10 mM $MgCl_2$) containing 200 μM of ATP. Parallel reactions were set without the addition of ATP to correct for background absorbance values. The absorbance at 360 nm was then measured at 20-s intervals for a total of 20 min at the physiological temperature of 37°C or 42°C for heat induction. The amount of inorganic phosphate released was quantified based on a KH_2PO_4 standard curve of 0 to 80 μM set in 100 μl reaction buffer. All reactions were preformed in duplicate for each experiment.

Protein fluorescence spectroscopy. The intrinsic protein fluorescence was determined using the Edinburgh FLS-920 fluorometer. Protein samples were diluted to 62.5 μg/ml in buffer containing 20 mM HEPES, pH 7.5, 150 mM NaCl, 10 mM $MgCl_2$, and 1 mM DTT in the presence or absence of 2 mM ATP. The excitation wavelength was set at 295 nm, while fluorescence emission was monitored between 305 nm and 450 nm. The excitation and emission slits were set at 5 nm, and the measurements were performed using a high photomultiplier tube voltage setting. All measurements were performed at 20°C and corrected for background emission values. Four independent measurements were performed, each in triplicate, for each p97 protein variant.

Limited-proteolysis assay and Western blot detection. Proteolysis reactions were performed at 37°C in a total volume of 50 μl containing 5 μg of p97, 250 ng of trypsin, and reaction buffer (20 mM HEPES, pH 7.5, 150 mM NaCl, 10 mM $MgCl_2$, and 1 mM DTT) in the presence or absence of 1 mM ATP for the indicated time intervals. The reactions were terminated by the addition of 0.5 mM phenylmethylsulfonyl fluoride and the reaction mixtures were boiled in 1× sodium dodecyl sulfate (SDS) loading buffer. Samples were subsequently subjected to SDS-polyacrylamide gel electrophoresis (PAGE) and transferred to polyscreen polyvinylidene difluoride membranes (Perkin Elmer, Zaventem, Belgium). Following blocking in 5% nonfat milk, the membranes were incubated in a monoclonal anti-p97 antibody at a dilution of 1:1,000 (BD Transduction Laboratories, San Jose, CA) for 1 h at room temper-

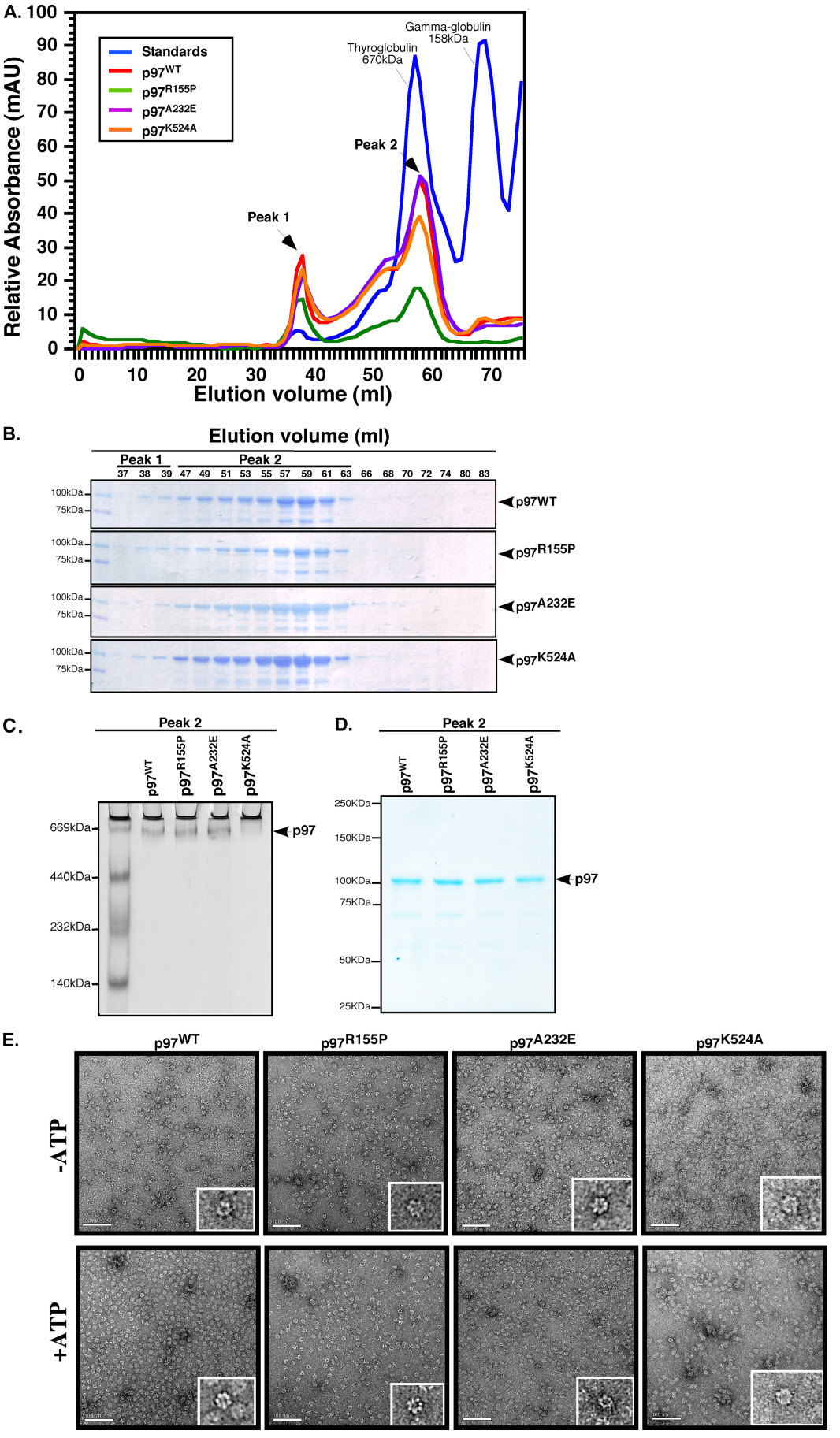

ature. The blots were then incubated in horseradish peroxidase-conjugated anti-mouse secondary antibody and subsequently developed using the ECL Plus detection system. Visualization was performed using the Storm 840 scanner (GE Healthcare, Baie d'Urfé, Canada).

Liquid chromatography-tandem mass spectrometry sequencing of full-length p97/VCP and limited-proteolysis products. Proteolysis reactions were performed by incubating 5 μg of $p97^{WT}$ with or without 250 ng of trypsin in buffer containing 20 mM HEPES, pH 7.5, 150 mM NaCl, 10 mM $MgCl_2$, 1 mM DTT, and 1 mM ATP. Reaction mixtures were set in 50 μl volumes and incubated at 37°C for 60 min. Following termination with 0.5 mM phenylmethylsulfonyl fluoride, samples were boiled in 1× SDS loading buffer and subjected to SDS-PAGE, followed by Coomassie staining. The stained bands were excised and analyzed at the Institut de Recherches Cliniques de Montréal proteomics discovery platform (Montréal, Canada).

Statistical analysis. Analysis of variance was conducted, followed by the Scheffé post hoc test or Tukey/Kramer analysis. Data were designated statistically significant only if the *P* value was equivalent to or less than 0.05. All tests were conducted using StatView 5.0 software (SAS Institute Inc., Cary, NC).

RESULTS

hIBMPFTD p97 mutants $p97^{R155P}$ and $p97^{A232E}$ form hexameric complexes similar to $p97^{WT}$ in vitro. To investigate the oligomerization patterns of $p97^{R155P}$ and $p97^{A232E}$, recombinantly expressed p97 proteins, first purified on a metal affinity column, were size fractionated by gel filtration chromatography (Fig. 1A and B). $p97^{WT}$, the hIBMPFTD mutants $p97^{R155P}$ and $p97^{A232E}$, and an ATPase-deficient mutant, $p97^{K524A}$, all eluted in two peaks: a minor peak within the void volume (Fig. 1A and B, peak 1) (~37 to 43 ml) and a major peak overlapping with the 670-kDa thyroglobulin complex (Fig. 1A and B, peak 2) (~47 to 63 ml). Further analysis of the major peak fraction by native gel electrophoresis also demonstrated that both $p97^{R155P}$ and $p97^{A232E}$ comigrated with $p97^{WT}$ and the thyroglobulin complex (Fig. 1C). Interestingly, $p97^{K524}$, which encompasses a mutation abolishing ATP binding in the D2 ring, could not be resolved under the native gel electrophoresis conditions used. These results indicate that $p97^{WT}$ and the hIBMPFTD mutants formed ~600-kDa complexes consistent with hexameric assembly. To confirm ring-shaped assembly, the hexameric protein peaks (Fig. 1D) were analyzed by negative-staining EM. At ×160,000 magnification, $p97^{R155P}$, $p97^{A232E}$, and $p97^{K524A}$ showed relatively homogeneous populations of ring-shaped particles notably similar to $p97^{WT}$ (Fig. 1E, top). ATP binding had no effect on the ring-shaped assembly of $p97^{WT}$ or mutant variants (Fig. 1E, bottom). Furthermore, all p97 protein samples contained some misfolded aggregates (not shown); however, there were no apparent differences in the structures or abundances of these aggregates between $p97^{WT}$ and the mutant variants. Altogether, these results confirm that the hIBMPFTD p97 mutants and $p97^{K524A}$ assemble into hexameric, ring-shaped complexes similar to $p97^{WT}$ and display no inherent propensity for misassembly or aggregation.

hIBMPFTD mutants $p97^{R155P}$ and $p97^{A232E}$ confer a gain-of-function phenotype on p97 total ATPase activity and alter its intrinsic fluorescence profile. The ATPase activities of $p97^{WT}$, $p97^{R155P}$, and $p97^{A232E}$ were monitored under physiological temperature and saturating ATP concentrations. At 37°C, $p97^{R155P}$ and $p97^{A232E}$ displayed significantly higher ATPase activity than $p97^{WT}$ (Fig. 2A and C and Table 1). The ATP hydrolysis rates of $p97^{R155P}$ and $p97^{A232E}$ were similar and about three times higher than the rate of $p97^{WT}$ (Fig. 2C and Table 1). At 42°C, there was no significant increase in $p97^{WT}$ ATPase activity; however, $p97^{R155P}$ and $p97^{A232E}$ displayed significant 1.7- and 1.4-fold increases, respectively (Fig. 2B and C and Table 1). Furthermore, $p97^{R155P}$'s heat-induced ATPase activity was significantly higher than that of $p97^{A232E}$ (Fig. 2C and Table 1). In contrast, $p97^{K524A}$ displayed no measurable ATPase activity at either temperature (Fig. 2A to C and Table 1). Collectively, these data show that the hIBMPFTD mutants $p97^{R155P}$ and $p97^{A232E}$ display not only elevated ATPase activity, but also increased sensitivity to heat-induced upregulation of ATPase activity.

To investigate if the upregulation in p97 ATPase activity was correlated with changes in the conformational state of the AAA^+ rings, a qualitative analysis was performed using intrinsic protein fluorescence spectroscopy (Fig. 3 and Table 2). In this assay, the change in protein fluorescence is inversely related to the hydrophobicity of tryptophan 476 (Trp^{476}) within the D2 ring (27). In the absence of ATP binding, only $p97^{R155P}$ showed significantly higher total fluorescence emission than $p97^{WT}$, which is indicative of increased basal accessibility of Trp^{476} (Table 2 and Fig. 3A). Both $p97^{A232E}$ and $p97^{K524A}$ also displayed higher total fluorescence emission than $p97^{WT}$, although it did not reach statistical significance (Table 2 and Fig. 3A). Upon ATP binding, $p97^{R155P}$ and $p97^{A232E}$ displayed significantly higher total fluorescence than $p97^{WT}$, which reflected increased solvent accessibility of Trp^{476} (Table 2 and Fig. 3B). On the other hand, $p97^{K524A}$ displayed significantly lower total fluorescence than $p97^{WT}$ and both hIBMPFTD-linked mutants, which is consistent with its inability to bind ATP in the D2 ring (Fig. 3B and C and Table 2). Comparison of the ATP-dependent changes in total fluorescence showed that $p97^{R155P}$ underwent the largest change in protein fluorescence (Fig. 3C and Table 2). Altogether, these data suggest that $p97^{R155P}$ undergoes the largest conformational change in response to ATP binding and that both $p97^{R155P}$ and $p97^{A232E}$ display ATP-dependent conformational alternations in the local region surrounding Trp^{476} within the D2 ring.

FIG. 1. Oligomeric assembly of p97/VCP and hIBMPFTD mutants. (A) Size exclusion chromatography of recombinant p97/VCP and mutant variants. Elution peaks for calibration controls, thyroglobulin and gamma globulin, are shown. Relative absorbance represents measured absorbance values at 280 nm adjusted for background absorbance. mAU, milli-absorbance units. (B) Coomassie blue staining of peak elutions from panel A. Fifty microliters of 1-ml elution fractions was loaded on 10% gels and subjected to SDS-PAGE. (C) Coomassie blue staining of $p97^{WT}$ or indicated mutants (5 μg) following native gel electrophoresis. (D) Coomassie blue staining of eluted p97/VCP proteins following size exclusion chromatography. $p97^{WT}$ or mutant variants (5 μg) were loaded on a 10% gel and resolved by SDS-PAGE. (E) Digital images of representative carbon grid fields containing p97/VCP particles with (+ATP) or without (−ATP) 1 mM ATP at ×160,000 magnification (scale bars, 100 nm). The insets show digitally enlarged p97/VCP particles.

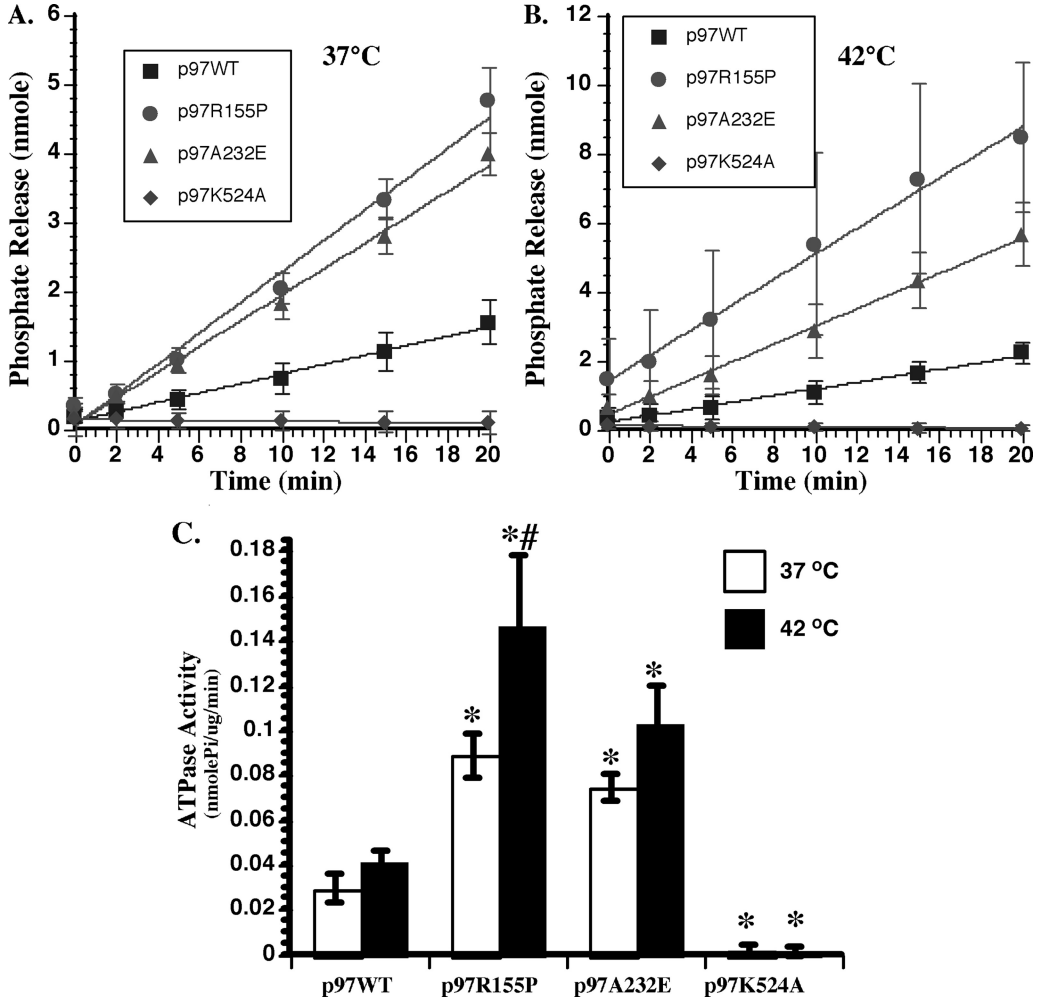

FIG. 2. ATPase activities of $p97^{WT}$ and hIBMPFTD mutants. (A and B) Quantification of ATP hydrolysis of $p97^{WT}$ or indicated mutants at selected time points. Measurements were performed at 37°C (A) or 42°C (B). (C) Quantification of the average ATP hydrolysis rates of $p97^{WT}$ or mutant variants. The data represent averages of at least four independent measurements with standard deviations. *, statistically significant compared to $p97^{WT}$ ($P \leq 0.05$).

hIBMPFTD mutants $p97^{R155P}$ and $p97^{A232E}$ display loss of the protective effect of ATP binding on D2 ring proteolysis. We further analyzed conformational differences between $p97^{WT}$ and the hIBMPFTD mutants using a limited-proteolysis approach. Trypsin-mediated digestion of full-length p97 generated two predominant cleavage products, p87 and p58, both retaining a large NH_2-terminal epitope (residues 9 to 130) (Fig. 4A). Silver stain analysis ruled out the presence of additional cleavage products (Fig. 4B).

TABLE 1. Quantification of p97/VCP ATPase activity

Protein	Activity (nmol P_i μg^{-1} min^{-1})	
	37°C	42°C
$p97^{WT}$	0.0289 ± 0.0065	0.0412 ± 0.0048
$p97^{R155P}$	0.0885 ± 0.0098[a]	0.1471 ± 0.0309[a,b]
$p97^{A232E}$	0.0742 ± 0.0058[a]	0.1036 ± 0.0156[a]
$p97^{K524A}$	0.0016 ± 0.0024[a]	0.0010 ± 0.0017[a]

[a] Statistically significant compared to $p97^{WT}$ (Tukey/Kramer test; $P \leq 0.05$).
[b] Statistically significant compared to $p97^{A232E}$ (Tukey/Kramer test; $P \leq 0.05$).

Thus, p87 reflected the cleavage of the COOH-terminal domain, while p58 resulted from additional proteolysis of the D2 ring. Comparison of proteolysis kinetics between $p97^{WT}$ and $p97^{R155P}$ revealed similar susceptibility patterns in the absence of ATP addition, while $p97^{A232E}$ and $p97^{K524A}$ were more prone to proteolysis (Fig. 4A, left). Specifically, p87 proteolysis was complete at 90 min for $p97^{A232E}$ and $p97^{K524A}$ compared to 120 min for $p97^{WT}$ and $p97^{R155P}$ (Fig. 4A and B, left). These data indicate that the conformation of the COOH-terminal domain and the D2 ring are more "labile" in $p97^{A232E}$ and $p97^{K524A}$. Furthermore, $p97^{WT}$ showed an ATP-dependent delay in p87 and p58 degradation in which both cleavage products could be detected 120 min after the initiation of the reaction (Fig. 4A, right). In contrast, p87 showed increased susceptibility to proteolytic cleavage in all p97 mutants, with $p97^{A232E}$ and $p97^{K524A}$ having the most accelerated degradation kinetics. Conversely, p58 was most strongly protected in $p97^{R155P}$ relative to all other p97 variants.

To identify the approximate sites of proteolysis, p97, p87, and p58 were sequenced using mass spectrometry (Table 3).

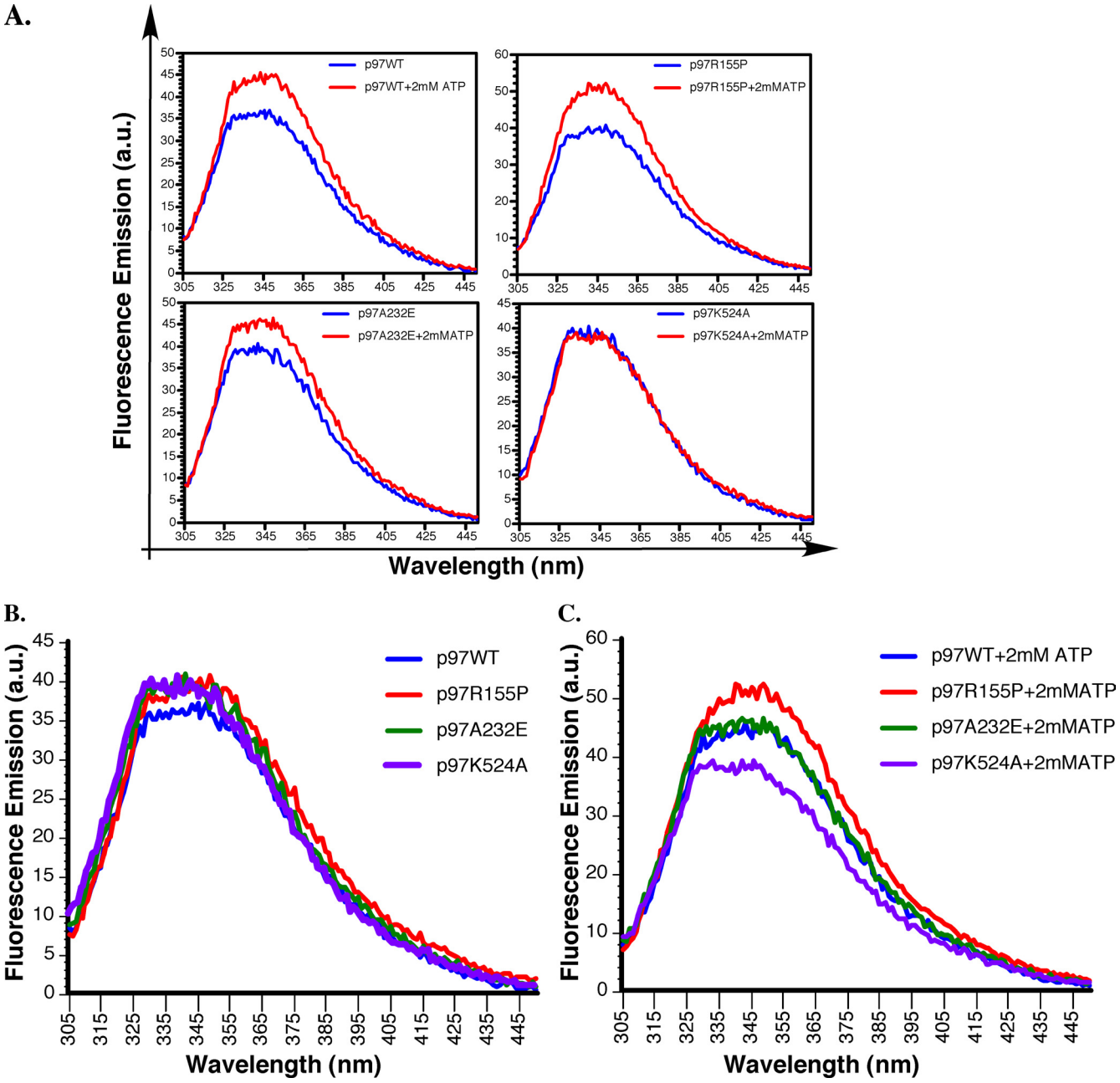

FIG. 3. Analysis of the intrinsic fluorescence properties of $p97^{WT}$ and hIBMPFTD mutants. (A) Fluorescence emission of $p97^{WT}$ or indicated mutants (62.5 μg/ml) between 305 and 450 nm, without nucleotide addition or in the presence of 2 mM ATP. (B) Comparison of $p97^{WT}$ or mutant p97 fluorescence emissions without nucleotide addition. (C) Comparison of $p97^{WT}$ or mutant p97 fluorescence emissions with 2 mM ATP. The data are representative of four measurements, each performed in triplicate. All measurements were corrected for background absorbance. a.u., arbitrary units.

TABLE 2. Comparison of p97/VCP total protein fluorescence emissions

Protein(s)	−ATP	+ATP	Δ
$p97^{WT}$	2,485.5 ± 89.6	3,025.9 ± 98.2	+540
$p97^{R155P}$	2,775.8 ± 126.9[a]	3,493.7 ± 99.0[a]	+717.9
$p97^{A232E}$	2,699.8 ± 169.3	3,141.3 ± 46.1[a]	+441.5
$p97^{K524A}$	2,663.1 ± 14.9	2,650.9 ± 76.6[a]	−12.2
$p97^{R155P}$ vs. $p97^{WT}$	+290.3 ± 99.8	+467.9 ± 48.9	
$p97^{A232E}$ vs. $p97^{WT}$	+214.3 ± 84.4	+115.4 ± 68.4	
$p97^{K524A}$ vs. $p97^{WT}$	−177.6 ± 94.5	−374.9 ± 34.3	

[a] Statistically significant compared to $p97^{WT}$ at a P value of ≤0.05 (Scheffe).

p97 sequencing resulted in the generation of peptides covering 58% of its total amino acid sequence. The most N-terminal amino acid residue was determined to be Gly^{9}, while Arg^{772} was identified as the last COOH-terminal residue. A large part of the COOH-terminal domain of p97 (residues 773 to 806) did not contain trypsin cleavage sites and therefore likely generated a peptide too large for detection by mass spectrometry (data not shown). Sequencing of p87 identified Leu^{26} in the NH_2-terminal domain and Arg^{709} at the COOH-terminal end,

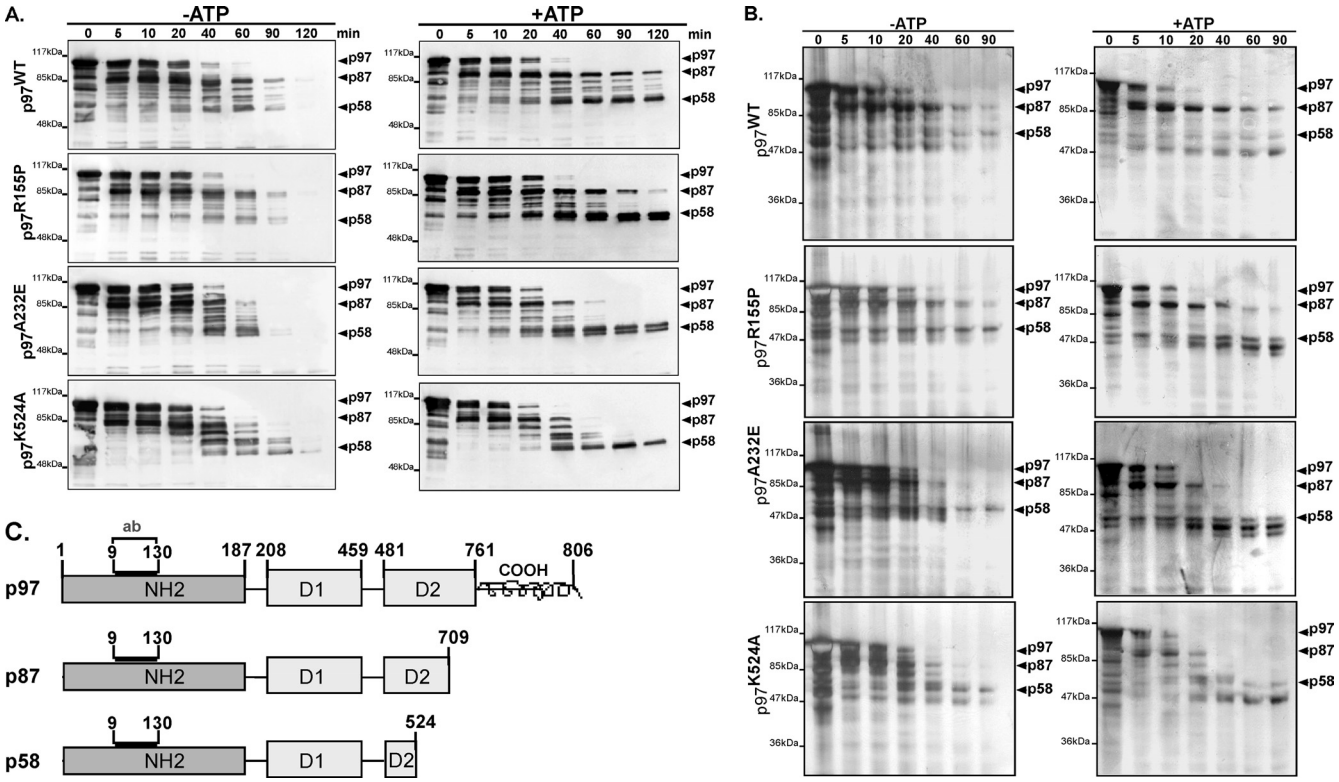

FIG. 4. Proteolysis kinetics of $p97^{WT}$ and hIBMPFTD mutants in a limited-proteolysis assay. (A) Western blot analysis of $p97^{WT}$ or mutant variants subjected to trypsin digestion for the indicated times, using a monoclonal anti-NH_2-terminal antibody (residues 9 to 130). (Left) Trypsin digestion without nucleotide addition. (Right) Trypsin digestion with 1 mM ATP. (B) Silver stain analysis of p97/VCP trypsinization kinetics with (right) or without (left) 1 mM ATP. (C) Schematic representation of p97/VCP fragments generated from trypsinization. ab, antibody; NH2, NH_2-terminal domain; D1, D1 cassette; D2, D2 cassette; COOH, carboxyl-terminal domain.

while the peptide coverage was determined to be 51% of the p97 total amino acid sequence. p58 sequencing covered 39% of the p97 amino acid sequence, starting with Met^{46} and ending with Lys^{524} (Table 3). These results suggest that the increased proteolytic susceptibility of p87 in $p97^{R155P}$ and $p97^{A232E}$ is due to D2 ring destabilization between residues Lys^{524} and Arg^{709} (Fig. 4C).

hIBMPFTD p97 mutants, $p97^{R155P}$ and $p97^{A232E}$, undergo ATP-dependent alteration in solution structure. In the absence of ATP, p97 particle size distribution consisted of two populations: a population of ~20-nm particles corresponding to assembled p97 (Fig. 5A and Table 4, peak 1) and a minor population reflecting large-diameter species (Fig. 5A and Table 4, peak 2). $p97^{R155P}$ and $p97^{A232E}$ showed distributions similar to that of $p97^{WT}$ (Fig. 5A) and displayed no significant differences in the estimated diameter of either assembled p97 or the large-diameter species (Table 4). In all cases, the most abundant population reflected hexameric p97 and accounted for at least 80% of the total light-scattering intensity (Table 4, peak 1). Interestingly, assembled $p97^{K524}$ and its large-diameter species both displayed significantly larger estimated diameters, with the assembled population accounting for at least 90% of the light-scattering intensity (Fig. 5A and Table 4, peak1 and peak 2).

In the presence of physiologically relevant ATP concentrations, there were no significant changes in the solution structure of $p97^{WT}$. In comparison, the light-scattering intensity of assembled $p97^{R155P}$ was significant reduced, and this effect correlated with an increase in the scattering intensity of the large-diameter population (Fig. 5B and Table 4). These results show an ATP-dependent shift toward increased abundance of the large-diameter population in $p97^{R155P}$. Furthermore, the estimated diameter of assembled $p97^{R155P}$ was significantly reduced compared to $p97^{WT}$ (Table 4). Similarly, $p97^{A232E}$ displayed a pronounced increase in the abundance of the large-diameter population, which was correlated with a significant reduction in particle size (Fig. 5B and Table 4). However, unlike $p97^{R155P}$, the diameter of assembled $p97^{A232E}$ was significantly reduced compared to the ATP-unbound state, as well as assembled $p97^{WT}$ (Table 4). These effects were correlated with a significant increase in the heterogeneity of the population's size distribution profile, as reflected in the increased polydispersity index estimate (Table 4). Therefore, ATP bind-

TABLE 3. Liquid chromatography-tandem mass spectrometry sequencing of p97/VCP tryptic fragments

Gel band	% Coverage of p97	Start residue	End Residue	Theoretical mass (kDa)	Functional domains
p97	58	Gly^{9}	Arg^{772}	85.4	NH_2-D1-D2
p87	51	Lys^{26}	Arg^{709}	75.9	NH_2-D1-partial D2
p58	39	Met^{45}	Lys^{524}	53.5	NH_2-D1-partial D2

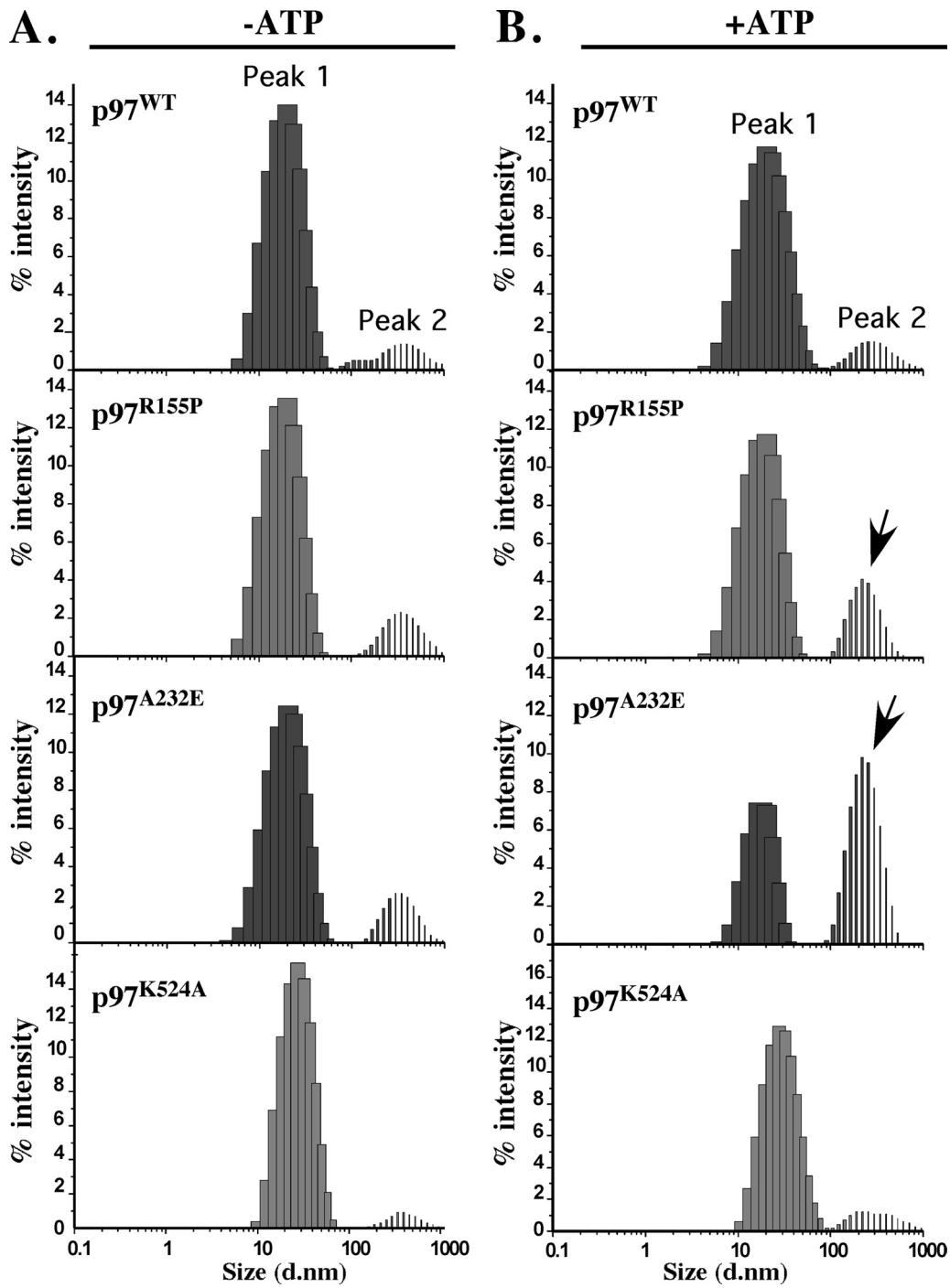

FIG. 5. Analysis of p97 particle size distribution in solution using DLS. Shown are average intensity size distributions of $p97^{WT}$ or mutant variants (100 μg/ml) without nucleotide addition (A) or with 1 mM ATP (B). The data represent averages of four measurements. The arrows point to high-molecular-weight intermediates statistically significant compared to $p97^{WT}$ ($P \leq 0.05$). d.nm, diameter in nanometers.

ing changed the solution structure of $p97^{A232E}$ and promoted the formation of large-diameter complexes. Moreover, the large-diameter population in $p97^{K524A}$ displayed changes similar to those in $p97^{A232E}$; however, despite the increased abundance of the large-diameter population in $p97^{K524A}$, both the size and light-scattering intensity were not significantly different from those of $p97^{WT}$ (Table 4). Interestingly, compared to $p97^{WT}$, ATP binding significantly reduced the diameters of assembled $p97^{R155P}$ and $p97^{A232E}$ but increased the diameter of $p97^{K524A}$ (Table 4). Altogether, these data provide evidence for ATP-dependent alterations in the solution structure of hIBMPFTD mutants and indicate that ATP binding may facilitate the formation of large-diameter species.

TABLE 4. Comparative analysis of p97/VCP particle size distribution in solution using DLS

Protein	Polydispersity index (arbitrary unit)	Peak 1		Peak 2	
		Diam (nm)	Intensity (%)	Diam(nm)	Intensity (%)
−ATP					
$p97^{WT}$	0.380 ± 0.04	22.73 ± 1.89	84.1 ± 2.5	413.5 ± 92.5	15.9 ± 2.5
$p97^{R155P}$	0.433 ± 0.03	21.80 ± 0.37	81.9 ± 2.7	384.1 ± 99.9	18.1 ± 2.7
$p97^{A232E}$	0.453 ± 0.01	23.47 ± 0.43	80.8 ± 0.7	345.1 ± 21.8	19.1 ± 0.8
$p97^{K524A}$	0.329 ± 0.02	30.75 ± 1.49[a]	95.8 ± 4.2[a]	734.0 ± 148[a]	4.20 ± 1.1[a]
+ATP					
$p97^{WT}$	0.343 ± 0.013	25.25 ± 0.97	87.4 ± 1.9	311.4 ± 116.2	12.5 ± 1.9
$p97^{R155P}$	0.459 ± 0.122	22.13 ± 0.70[a]	71.1 ± 1.7[a]	236.5 ± 26.06	28.8 ± 2.1[a]
$p97^{A232E}$	0.954 ± 0.080[a]	20.11 ± 0.12[a]	35.0 ± 2.0[a]	239.5 ± 16.65	65.0 ± 2.0[a]
$p97^{K524A}$	0.333 ± 0.013	34.55 ± 0.66[a]	87.2 ± 1.1	403.3 ± 130.0	12.8 ± 1.1

[a] Statistically significant from $p97^{WT}$ at $P \leq 0.05$ (Scheffe).

DISCUSSION

hIBMPFTD is a degenerative disorder caused by single substitutions in highly conserved amino acid residues in the NH_2 domain and the D1 ring of p97/VCP (13, 28). The affected residues are proposed to play roles in relaying conformational changes initiated in the D2 ring to adaptor protein complexes (5). These ATP-powered conformational changes (21, 22), in turn, provide the mechanistic basis for p97 cell biological activity. In this study, we provide evidence for structural defects in the hIBMPFTD p97 mutants $p97^{R155P}$ and $p97^{A232E}$. We show that both mutations upregulate p97 ATPase activity and increase sensitivity to heat-induced upregulation of ATPase activity. Using protein fluorescence analysis and a limited-proteolysis assay, we provide evidence for altered conformational states and destabilization of the D2 ring. We further show that these defects are correlated with a propensity for nucleotide-dependent aggregation of both mutants in solution. Based on these data, we propose that structural defects in p97/VCP may underlie the pathogenesis of hIBMPFTD.

hIBMPFTD p97/VCP mutations in Arg^{155} and Ala^{232} do not impair spontaneous self-assembly. Using size exclusion chromatography and native gel electrophoresis, we showed that hIBMPFTD mutants $p97^{R155P}$ and $p97^{A232E}$ assembled into hexameric complexes and ruled out the possibility of misassembly or deoligomerization. Visualization by EM further confirmed the ring-shaped structure of the pathogenic p97 mutants. These results are in agreement with a previous finding that $p97^{R155H}$ does not display an oligomerization defect (30) and are consistent with the NH_2 domain being dispensable for hexamerization (22, 33). We also showed that the p97 mutation A232E does not impair hexamerization, in spite of its localization in the D1 ring, which is necessary for p97 self-assembly (26). Residue Ala^{232} is positioned at the junction between the D1 domain and the NH_2-D1 linker region (28). This peripheral localization is inconsistent with a role in regulating interprotomer interaction within the D1 ring. Other works have demonstrated that p97 oligomerization is spontaneous and that nucleotide binding to the D1 ring stabilizes the hexamer (26). The only single-amino-acid mutations known to prevent p97/VCP assembly affect the D1 Walker A residue, Lys^{251} (6, 25), or the D1 second region of homology residue, Arg^{362} (25). Mutations of residues lining the D1 pore (Arg^{313}, Lys^{315}, Thr^{316}, His^{317}, Glu^{319}, and Arg^{322}) also do not influence oligomerization (6). Together, our results suggest that the disease severity associated with mutation in Ala^{232} in hIBMPFTD is likely unrelated to an oligomerization defect in p97/VCP. Interestingly, our data also suggest that $p97^{K524A}$ may form higher ring-shaped oligomers than $p97^{WT}$ or hIBMPFTD mutant variants. This is evident in its migration pattern on native gel electrophoresis and its significantly larger estimated diameter in solution. Recent work has demonstrated that the D2 ring adopts a heptameric structure with a sevenfold symmetry when purified independently of the NH_2 domain and the D1 ring (3). It is possible that disrupting nucleotide binding in the D2 ring may also alter the fold symmetry of p97/VCP. Alternatively, the $p97^{K524A}$ mutation may alter the shape of the hexamer in a way that influences its native gel migration and increases its apparent diameter in solution.

hIBMPFTD p97 mutants $p97^{R155P}$ and $p97^{A232E}$ show increased ATPase activity. Under the conditions used, the specific ATPase activity of $p97^{WT}$ was lower than the values previously reported (6, 14, 24), although different expression, purification, and assay conditions were used. Nevertheless, our data show an ~3-fold increase in $p97^{R155P}$ ATPase activities. In another report, the $p97^{R155H}$ mutant displayed ATPase activity levels comparable to those of $p97^{WT}$, whereas heat-induced upregulation in ATPase activity was not assessed (30). One explanation for this discrepancy is the nature of the amino acid change associated with Arg^{155}. For example, DeLaBarre and colleagues showed that different amino acid substitutions for the D1 pore residue His^{317} could have opposing effects on p97 ATPase activity, in spite of the fact that His^{317} is not directly involved in ATP binding or hydrolysis (6). Nevertheless, our results pose the possibility that the p97 NH_2 domain is involved in the positive regulation of p97 basal ATPase activity. The strong ATP-dependent protection of the p58 N-terminal fragment of $p97^{R155P}$ in the limited-proteolysis assay suggests increased affinity for ATP binding in the D1 ring. Changes in nucleotide-binding affinity may alter the cooperativity between the D1 and D2 rings. Furthermore, previous studies demonstrated that some adaptor proteins binding to the p97 NH_2 domain (i.e., p47) downregulate p97 ATPase activity (14), while others had no effect (i.e., Npl4/Ufd1) (2). It remains to be determined whether any of the p97 ubiquitous NH_2 domain binding proteins could play a role in the positive regulation of its ATPase activity. Interestingly, deletion of

the NH_2 terminus does not influence p97 ATPase activity (20, 22, 33).

Our results also show that, like $p97^{R155P}$, $p97^{A232E}$ displayed upregulated ATPase activity. The contribution of the D1 ring to p97 basal ATPase activity is unclear (24, 33); however, it is known to be activated in response to heat stimulation (24). Our data show that the ATPase activities of both mutants are significantly upregulated at 42°C but do not rule out the ectopic activation of the D1 ring at 37°C. Accordingly, this increase in basal ATPase activity could be attributed to either D1 ring activation at 37°C or increased activity of the D2 ring, or both. On the other hand, the increased sensitivity to heat stimulation suggests alteration in the D1 ring function. Nevertheless, an increase in ATPase activity may detrimentally alter p97 cell biological activities by destabilizing p97-mediated protein interactions or, alternatively, by leading to the gain of new toxic functions (i.e., increasing binding affinity or promiscuity of p97/VCP-substrate interaction). Further studies are needed to address the mechanism by which hIBMPFTD mutations upregulate p97 ATPase activity and the possible implications for biological systems.

Evidence of structural defects in hIBMPFTD p97/VCP mutants $p97^{R155P}$ and $p97^{A232E}$. Our results indicate that the Arg^{155} and Ala^{232} mutations influence distant residues within the p97 structure, a fact consistent with the dynamic nature of p97 interdomain communication (21, 22). Considering that Trp^{476} fluorescence has been used to report ATP-dependent conformational changes within the D2 ring (27), our data suggest that $p97^{R155P}$ and $p97^{A232E}$ display different D2 ring conformations than $p97^{WT}$. We further defined the affected region between residues Lys^{524} and Arg^{709}, which covers part of the D2 ring and the COOH-terminal domain. The tryptic proteolysis assay showed that this region is more susceptible to proteolysis. Wang et al. previously demonstrated that $p97^{WT}$ showed a large increase in protein fluorescence in response to ATP binding and that this was correlated with protection of the D2 ring from proteolysis (27). While this is consistent with the results reported here, both $p97^{R155P}$ and $p97^{A232E}$ showed significantly higher ATP-dependent shifts in protein fluorescence than $p97^{WT}$ with only partial D2 ring protection during the limited-proteolysis assay. It is possible that an elevated rate of nucleotide exchange may account for the increased proteolytic susceptibility of the D2 ring, especially since the p97 D2 ring adopts a flexible state directly following nucleotide release (5). Alternatively, the increased ATPase activity may be consequential to structural defects imposed by mutations in residues Arg^{155} and Ala^{232}. In either case, the results indicate that the ATP-bound D2 ring adopts a relaxed conformation in $p97^{R155P}$ and $p97^{A232E}$ compared $p97^{WT}$.

Interestingly, while $p97^{R155P}$ displayed a larger change in protein fluorescence than $p97^{A232E}$, it was not correlated with faster proteolysis kinetics.

A possible explanation is that the Arg^{155} mutation increases the affinity for nucleotide binding, as suggested by the strong protection of p58 during the limited-proteolysis assay. Nevertheless, both $p97^{R155P}$ and $p97^{A232E}$ showed increased proteolytic susceptibility in the region between residues Lys^{524} and Arg^{709}. Importantly, this region contains residues central to p97 function in ER-associated degradation (ERAD), specifically Arg^{586} and Arg^{599}, as well as Phe^{551} and Trp^{552} (6). Arg^{586}/Arg^{599} have been suggested to form a "denaturation collar" for the processing of misfolded ERAD substrates, and Phe^{551}/Trp^{552} have been proposed to bind to misfolded substrates through hydrophobic interactions (8, 27). It is also known that Arg^{586}/Arg^{599} adopt different localizations relative to the D2 pore during the ATPase cycle (5). Thus, the conformational integrity of the D2 ring is necessary for proper substrate processing, and its perturbation in hIBMPFTD mutations may represent a possible mechanism of pathogenesis. Although it is still unclear if hIBMPFTD-linked p97 mutations influence the accessibility or function of the "denaturation collar," our data indicate that the overall conformational state of the D2 ring is altered in mutant p97 complexes. Indeed, hIBMPFTD-linked mutation in residue Arg155 (R155H) has been shown to impair the degradation of the ERAD substrate, ΔF508-CFTR (cystic fibrosis transmembrane conductance regulator), in C2C12 skeletal myoblasts (30). Future studies are necessary to substantiate whether all hIBMPFTD-linked p97 mutations result in similar alterations in the D2 ring conformation and if this is indeed a relevant mechanism of pathogenesis in vivo.

Consequences of hIBMPFTD mutations for the p97/VCP solution structure. DLS is a technique used to resolve particle size distribution in solution. Our analysis clearly showed a didispersed distribution consisted of assembled p97/VCP and large-diameter species. The hydrated diameter of p97, estimated at 20 to 25 nm, is consistent with published structural data (22). Remarkably, we showed an ATP-dependent increase in the light-scattering intensity of the large-diameter population in samples containing $p97^{R155P}$ and $p97^{A232E}$, but not $p97^{WT}$ or $p97^{K524A}$. Considering that there was no significant increase in diameter, the increase in the light-scattering intensity should be attributed to increased abundance of the large-diameter species. This finding appears at odds with our EM images, which show assembled, ring-shaped p97/VCP in the presence of ATP. However, it is important to note that the percent intensity measurements in DLS do not reflect the actual proportion of the large-diameter species versus hexameric p97 particles and that DLS detects large-diameter species with high sensitivity. Overall, based on the EM study and the ATPase activity analyses, we conclude that hexameric $p97^{R155P}$ and $p97^{A232E}$ remain the predominant populations. However, in solution, $p97^{R155P}$ and $p97^{A232E}$ show an ATP-dependent propensity to assemble into large-diameter particles. The fact that the estimated diameter of these particles was ~10 times larger than the diameter of the assembled hexamers poses the possibility of ATP-mediated aggregate formation. Alternatively, the large-diameter particles may represent a population of transiently interacting p97 hexamers.

Together, these biochemical data provide the first evidence of structural defects associated with hIBMPFTD p97 mutations. Importantly, these defects were correlated with increased ATPase activity and alterations in the mutant p97 solution structure. It remains unclear whether these defects could be generalized to other hIBMPFTD p97 mutations, especially since both mutations, R155P and A232E, are relatively rare (13). It is known that some p97 mutants, such as $p97^{R95G}$ and $p97^{R155H}$, show reduced solubility in cell culture models (30). Consistently, our initial analysis of $p97^{R95G}$ expression in recombinant expression systems also showed reduced solubility

(unpublished data). Thus, it remains to be seen if this effect is secondary to structural and biochemical defects such as those reported here. We propose that hIBMPFTD mutations influence the D2 ring conformation by increasing its flexibility and reducing its compactness upon ATP binding. Considering the newly proposed role of the D2 ring in the processing of protein substrates (6, 8), these defects may have detrimental consequences for p97 cell biological functions.

ACKNOWLEDGMENTS

We gratefully acknowledge Tom Rapoport (Harvard University, Cambridge, MA) and Yihong Ye (NIDDK, NIH, Bethesda, MD) for the initial cloning of the ATPase-deficient $p97^{K524A}$ construct and for their generous advice on the expression and purification of recombinant p97. We also thank Julie Jodoin (McGill University, Montréal, QC, Canada) for advice on the statistical analysis and critical reading of the manuscript, Julia Guy (University of Montréal, Montréal, QC, Canada) for assistance with the fluorometeric analysis, and Archana Srivastava for assistance with the EM imaging.

Part of this work was supported by grants from the HFSP, Genome Canada, Silicon Kinetics, and Genocean to M.L.; CIHR grant MOP-86693 to I.R.; CIHR grant MOP-53282 to M.J.S.; and CIHR grant MOP-81146 to A.L. I.R. is the recipient of a CIHR New Investigator award, and M.J.S. is the recipient of an Rx&D/CIHR Health Research Foundation Career Award in Health Sciences. M.L. acknowledges support from the Canada Research Chair Program.

REFERENCES

1. **Acharya, U., R. Jacobs, J. M. Peters, N. Watson, M. G. Farquhar, and V. Malhotra.** 1995. The formation of Golgi stacks from vesiculated Golgi membranes requires two distinct fusion events. Cell **82:**895–904.
2. **Bruderer, R. M., C. Brasseur, and H. H. Meyer.** 2004. The AAA ATPase p97/VCP interacts with its alternative co-factors, Ufd1-Npl4 and p47, through a common bipartite binding mechanism. J. Biol. Chem. **279:**49609–49616.
3. **Davies, J. M., A. T. Brunger, and W. I. Weis.** 2008. Improved structures of full-length p97, an AAA ATPase: implications for mechanisms of nucleotide-dependent conformational change. Structure **16:**715–726.
4. **DeLaBarre, B., and A. T. Brunger.** 2003. Complete structure of p97/valosin-containing protein reveals communication between nucleotide domains. Nat. Struct. Biol. **10:**856–863.
5. **DeLaBarre, B., and A. T. Brunger.** 2005. Nucleotide dependent motion and mechanism of action of p97/VCP. J. Mol. Biol. **347:**437–452.
6. **DeLaBarre, B., J. C. Christianson, R. R. Kopito, and A. T. Brunger.** 2006. Central pore residues mediate the p97/VCP activity required for ERAD. Mol. Cell **22:**451–462.
7. **Forman, M. S., I. R. Mackenzie, N. J. Cairns, E. Swanson, P. J. Boyer, D. A. Drachman, B. S. Jhaveri, J. H. Karlawish, A. Pestronk, T. W. Smith, P. H. Tu, G. D. Watts, W. R. Markesbery, C. D. Smith, and V. E. Kimonis.** 2006. Novel ubiquitin neuropathology in frontotemporal dementia with valosin-containing protein gene mutations. J. Neuropathol. Exp. Neurol. **65:**571–581.
8. **Halawani, D., and M. Latterich.** 2006. p97: the cell's molecular purgatory? Mol. Cell **22:**713–717.
9. **Hubbers, C. U., C. S. Clemen, K. Kesper, A. Boddrich, A. Hofmann, O. Kamarainen, K. Tolksdorf, M. Stumpf, J. Reichelt, U. Roth, S. Krause, G. Watts, V. Kimonis, M. P. Wattjes, J. Reimann, D. R. Thal, K. Biermann, B. O. Evert, H. Lochmuller, E. E. Wanker, B. G. Schoser, A. A. Noegel, and R. Schroder.** 2007. Pathological consequences of VCP mutations on human striated muscle. Brain **130:**381–393.
10. **Indig, F. E., J. J. Partridge, C. von Kobbe, M. I. Aladjem, M. Latterich, and V. A. Bohr.** 2004. Werner syndrome protein directly binds to the AAA ATPase p97/VCP in an ATP-dependent fashion. J. Struct. Biol. **146:**251–259.
11. **Jentsch, S., and S. Rumpf.** 2007. Cdc48 (p97): a "molecular gearbox" in the ubiquitin pathway? Trends Biochem. Sci. **32:**6–11.
12. **Ju, J. S., S. E. Miller, P. I. Hanson, and C. C. Weihl.** 2008. Impaired protein aggregate handling and clearance underlie the pathogenesis of p97/VCP-associated disease. J. Biol. Chem. **283:**30289–30299.
13. **Kimonis, V. E., E. Fulchiero, J. Vesa, and G. Watts.** 2008. VCP disease associated with myopathy, Paget disease of bone and frontotemporal dementia: review of a unique disorder. Biochim. Biophys. Acta **1782:**744–748.
14. **Meyer, H. H., H. Kondo, and G. Warren.** 1998. The p47 co-factor regulates the ATPase activity of the membrane fusion protein, p97. FEBS Lett. **437:**255–257.
15. **Neumann, M., I. R. Mackenzie, N. J. Cairns, P. J. Boyer, W. R. Markesbery, C. D. Smith, J. P. Taylor, H. A. Kretzschmar, V. E. Kimonis, and M. S. Forman.** 2007. TDP-43 in the ubiquitin pathology of frontotemporal dementia with VCP gene mutations. J. Neuropathol. Exp. Neurol. **66:**152–157.
16. **Partridge, J. J., J. O. Lopreiato, Jr., M. Latterich, and F. E. Indig.** 2003. DNA damage modulates nucleolar interaction of the Werner protein with the AAA ATPase p97/VCP. Mol. Biol. Cell **14:**4221–4229.
17. **Pye, V. E., I. Dreveny, L. C. Briggs, C. Sands, F. Beuron, X. Zhang, and P. S. Freemont.** 2006. Going through the motions: the ATPase cycle of p97. J. Struct. Biol. **156:**12–28.
18. **Rabouille, C., T. P. Levine, J. M. Peters, and G. Warren.** 1995. An NSF-like ATPase, p97, and NSF mediate cisternal regrowth from mitotic Golgi fragments. Cell **82:**905–914.
19. **Rape, M., T. Hoppe, I. Gorr, M. Kalocay, H. Richly, and S. Jentsch.** 2001. Mobilization of processed, membrane-tethered SPT23 transcription factor by CDC48(UFD1/NPL4), a ubiquitin-selective chaperone. Cell **107:**667–677.
20. **Rothballer, A., N. Tzvetkov, and P. Zwickl.** 2007. Mutations in p97/VCP induce unfolding activity. FEBS Lett. **581:**1197–1201.
21. **Rouiller, I., V. M. Butel, M. Latterich, R. A. Milligan, and E. M. Wilson-Kubalek.** 2000. A major conformational change in p97 AAA ATPase upon ATP binding. Mol. Cell **6:**1485–1490.
22. **Rouiller, I., B. DeLaBarre, A. P. May, W. I. Weis, A. T. Brunger, R. A. Milligan, and E. M. Wilson-Kubalek.** 2002. Conformational changes of the multifunction p97 AAA ATPase during its ATPase cycle. Nat. Struct. Biol. **9:**950–957.
23. **Schroder, R., G. D. Watts, S. G. Mehta, B. O. Evert, P. Broich, K. Fliessbach, K. Pauls, V. H. Hans, V. Kimonis, and D. R. Thal.** 2005. Mutant valosin-containing protein causes a novel type of frontotemporal dementia. Ann. Neurol. **57:**457–461.
24. **Song, C., Q. Wang, and C. C. Li.** 2003. ATPase activity of p97-valosin-containing protein (VCP). D2 mediates the major enzyme activity, and D1 contributes to the heat-induced activity. J. Biol. Chem. **278:**3648–3655.
25. **Wang, Q., C. Song, L. Irizarry, R. Dai, X. Zhang, and C. C. Li.** 2005. Multifunctional roles of the conserved Arg residues in the second region of homology of p97/valosin-containing protein. J. Biol. Chem. **280:**40515–40523.
26. **Wang, Q., C. Song, and C. C. Li.** 2003. Hexamerization of p97-VCP is promoted by ATP binding to the D1 domain and required for ATPase and biological activities. Biochem. Biophys. Res. Commun. **300:**253–260.
27. **Wang, Q., C. Song, X. Yang, and C. C. Li.** 2003. D1 ring is stable and nucleotide-independent, whereas D2 ring undergoes major conformational changes during the ATPase cycle of p97-VCP. J. Biol. Chem. **278:**32784–32793.
28. **Watts, G. D., J. Wymer, M. J. Kovach, S. G. Mehta, S. Mumm, D. Darvish, A. Pestronk, M. P. Whyte, and V. E. Kimonis.** 2004. Inclusion body myopathy associated with Paget disease of bone and frontotemporal dementia is caused by mutant valosin-containing protein. Nat. Genet. **36:**377–381.
29. **Webb, M. R.** 1992. A continuous spectrophotometric assay for inorganic phosphate and for measuring phosphate release kinetics in biological systems. Proc. Natl. Acad. Sci. USA **89:**4884–4887.
30. **Weihl, C. C., S. Dalal, A. Pestronk, and P. I. Hanson.** 2006. Inclusion body myopathy-associated mutations in p97/VCP impair endoplasmic reticulum-associated degradation. Hum. Mol. Genet. **15:**189–199.
31. **Weihl, C. C., S. E. Miller, P. I. Hanson, and A. Pestronk.** 2007. Transgenic expression of inclusion body myopathy associated mutant p97/VCP causes weakness and ubiquitinated protein inclusions in mice. Hum. Mol. Genet. **16:**919–928.
32. **Weihl, C. C., P. Temiz, S. E. Miller, G. Watts, C. Smith, M. Forman, P. I. Hanson, V. Kimonis, and A. Pestronk.** 2008. TDP-43 accumulation in inclusion body myopathy muscle suggests a common pathogenic mechanism with frontotemporal dementia. J. Neurol. Neurosurg. Psychiatry **79:**1186–1189.
33. **Ye, Y., H. H. Meyer, and T. A. Rapoport.** 2003. Function of the p97-Ufd1-Npl4 complex in retrotranslocation from the ER to the cytosol: dual recognition of nonubiquitinated polypeptide segments and polyubiquitin chains. J. Cell Biol. **162:**71–84.